Check for updates

Sustainable castor oil-derived cross-linked poly(ester-urethane) elastomeric films for stretchable transparent conductive electrodes and heaters†

Timo Laukkanen, ‡[a] Pulikanti Guruprasad Reddy, ‡*[a] Amit Barua,[a] Manish Kumar,[a] Kristofer Kolpakov,[a] Teija Tirri[b] and Vipul Sharma *[a]

Substrates are essential for flexible and stretchable devices, requiring sustainability, stretchability, transparency, thermal stability, and chemical stability. This study introduces a sustainable cross-linked poly(castor oil-*co*-δ-valerolactone)cyclohexyl urethane (PCVU) substrate for flexible, stretchable transparent conducting electrodes (TCEs) based strain sensors and heaters. PCVU is synthesized as a highly transparent (>90%), stretchable (>190%), and thermally stable (~210 °C) substrate *via* thermal cross-link polymerization of poly(castor oil-*co*-δ-valerolactone)triol and 4,4′-methylenebis(cyclohexyl isocyanate) on a glass mold. PCVU exhibits high chemical stability in various organic solvents and good degradability in acidic (pH 0, 45% degradation), alkaline (pH 14, 100% degradation), and phosphate buffer (pH 7.2, 9% degradation) aqueous solutions over 150 days. Using PCVU, we fabricated a robust, flexible, and stretchable TCE with low sheet resistance (<50 Ω sq^{-1}). The TCE fabrication process involves applying an electrospun polyvinyl alcohol (PVA) layer as a temporary wet film leveling agent to improve the dispersion and adhesion of silver nanowires (AgNWs) on PCVU films, followed by a heat-based nano-welding technique to enhance the durability and mechanical stability of the TCE. The TCE-based strain sensor showed stable and repeatable resistance changes ($\Delta R/R_0$) under 5–15% strains, with fast response and consistent signal stability over 100 cycles at 5% strain. The flexible heater reached a maximum average temperature of ~150 °C at 5.5 V, with rapid heating and cooling responses (15 s each). Practical applications include a strain sensor for real-time monitoring of human motion (finger, wrist, elbow, and neck flexion) and a heater used as a thermotherapy pad for the wrist and finger, demonstrating the potential of PCVU-based TCEs for wearable and medical devices.

1. Introduction

In recent years, flexible and stretchable electronics have gained significant attention due to their potential applications in health technology, human–machine interfaces, flexible and stretchable displays, optoelectronics, soft robotics, solar energy, and other Internet of Things (IoT).[1–4] The performance of these devices relies on the use of flexible Transparent Conducting Electrodes (TCEs), which enable the transmission of electrical signals and energy through transparent, stretchable materials.[2,5] In the medical field, transparency is sometimes important, and flexible TCEs are crucial because they improve patient monitoring by monitoring the healing and treatment processes. These devices

enhance diagnostic capabilities when used in wearable technology. TCEs are widely used in wearable health monitors (such as smart patches and fitness trackers), electronic skins (e-skins), medical thermotherapy patches, and lab-on-a-chip devices for point-of-care testing (*e.g.*, diagnostic kits and chemical sensors), as well as implantable medical devices and smart medical clothing.[6–8] Particularly, e-skins are rapidly evolving due to their ability to conformally attach to the skin, enabling real-time health and disease monitoring.[7] Thus, the development of flexible TCEs is crucial for advancing health monitoring devices.

The performance of stretchable TCEs depends on their characteristics, including low sheet resistance, high transparency, durability, flexibility, adhesion, and sustainability. These characteristics are influenced by the choice of conductive nanomaterials, transparent substrates, and fabrication methods used. Traditional TCEs often utilize indium tin oxide (ITO) as a conductive layer, which meets high transmittance, and low sheet resistance requirements required in flexible electronics applications. However, it does not meet essential

*a*Department of Mechanical and Materials Engineering, University of Turku, Turku-20500, Finland. E-mail: guru.pulikanti@utu.fi; vipul.sharma@utu.fi

*b*Faculty of Science and Engineering, Åbo Akademi University, Turku-20500, Finland

† Electronic supplementary information (ESI) available. See DOI: https://doi.org/10.1039/d4ta05338a

‡ Both authors contributed equally.

This journal is © The Royal Society of Chemistry 2024

J. Mater. Chem. A, 2024, **12**, 33177–33192 | 33177

flexibility criteria due to its tendency to crack-based device failures, and concerns about toxicity, which limit its use in flexible devices.[8] As a result, research is increasingly exploring alternative conductive materials such as graphene, carbon nanotubes, metallic nanowires, and conducting polymers.[9–12] These materials offer mechanical flexibility, improved conductivity, potential cost reductions, and enhanced sustainability. Currently, metallic nanowires, particularly silver nanowires (AgNWs) are getting attention for their exceptional electrical conductivity and high optical transparency.[9,13] Their flexibility makes them highly suitable for the rapidly expanding field of flexible and wearable electronics.[14] However, a significant challenge in fabricating AgNW-based TCEs is their poor adhesion to the substrate,[15] which is crucial for maintaining mechanical durability and electrical performance. The poor adhesion is due to the weak van der Waals forces and limited contact area between AgNWs and the substrate, which often result in nanowire detachment during bending and stretching, resulting in failure of electrical connectivity and overall durability.[16] Current methods to improve adhesion include embedding AgNWs into polymeric substrates, using conductive cross-linked polymeric layers as adhesive promoters, applying metal oxide layers, and incorporating buffer-based thermal lamination layers, among others.[17–21] However, these methods are complex and can risk damaging the substrate and AgNWs, which adversely affects the performance and characteristics of TCEs. Additionally, the junction resistance of AgNWs poses another significant challenge, limiting the overall conductivity of TCEs. Techniques such as thermal annealing, chemical welding, cold welding, and laser-induced welding are employed to reduce junction resistance by effectively welding nanowires together.[13,22,23] Nevertheless, achieving mechanically robust TCEs that exhibit uniform and stable sheet resistance across their surface while maintaining decent transparency remains a formidable task. Therefore, innovative fabrication methods are urgently needed to address these challenges.

Recently, a variety of AgNW-based flexible TCEs for e-skins have been developed and used as tactile sensors, including capacitive pressure sensors, strain sensors, and curvature sensors.[24] These sensors are important in health technology, enabling real-time monitoring of human health by transducing external strains or pressures into electrical signals such as resistance and capacitance.[25,26] This is crucial for the early detection and diagnosis of health conditions through monitoring human motions in real-time. Additionally, they are beneficial in medical thermotherapy applications, functioning as thermotherapy pads (TTPs) to enhance blood circulation, reduce inflammation, and alleviate pain.[27–29] TTPs are particularly effective for treating diseases like rheumatoid arthritis, scapulohumeral periarthritis, cervical spondylosis, and various traumatic injuries.[28] However, advanced TCEs based e-skin requires a stretchable substrate that adheres conformally to human skin and is soft, lightweight, resilient to wear and tear, highly flexible, stretchable, transparent, chemically stable, thermally stable, and sustainable.[30–32] For TTPs, high thermal stability, transparency, and sustainability are especially critical parameters for the substrate.[27–29] Currently, a variety of

traditional stretchable elastomers like silicon-based elastomers (e.g., polydimethylsiloxane (PDMS), dragon skin, Ecoflex, Sylgard), thermoplastic polyurethanes (TPU), and styrene–ethylene–butylene–styrene (SEBS)[30–32] are used as stretchable and flexible substrates for e-skin fabrication. However, these materials face sustainability issues and contribute to electronic waste (e-waste) based flexible devices due to their non-degradability. These also encounter other challenges; for example, SEBS composite films (~144 °C),[33] TPUs (~130 °C)[34] and other silicone elastomers such as PDMS (~200 °C),[34] Ecoflex (~115 °C),[35] exhibit poor thermal properties unsuitable for flexible heaters. Additionally, all silicone-based elastomers display poor chemical resistance, swelling in the presence of organic solvents, which negatively impacts TCEs fabrication process.[36] Therefore, there is a high demand to develop alternative substrates that are not only environmentally friendly and degradable but also meet the rigorous performance requirements for e-skins and flexible heaters.

The current state-of-the-art in designing flexible TCEs involves a variety of sustainable substrates derived from natural plant-based materials (e.g., wood, leaf skeletons, pollen)[37] and biopolymers (e.g., cellulose,[38] starch, chitosan,[39] silk,[40] agarose gels).[41] These substrates are developed based on their availability, robustness and sustainability. However, TCEs derived from plant materials and biopolymers often exhibit poor mechanical properties and lack thermal and environmental stability. Conversely, several degradable synthetic elastomers are reported as sustainable substrates for flexible devices.[42–47] Despite their degradability, flexible conducting electrodes made from these elastomers often fall short in transparency and stretchability, and other fabrication challenges. Given these limitations, there is a need to develop innovative methodologies for sustainable substrates design along with novel fabrication methodologies to create sustainable and highly durable TCEs. Such advancements are crucial for developing environmentally responsible next-generation flexible devices for human health monitoring and human–machine interfaces. In previous years, our group has developed a series of sustainable TCEs using biotic substrates, exploring their use in flexible electronic devices including tactile sensors and flexible heaters.[27,48,49] Recently, we reported cross-linked poly(glycerol-urethane) elastomeric substrates and multi-purpose transparent electrodes for wearable electronic devices.[50] The flexible and transparent TCEs made from these substrates demonstrated versatility as capacitive pressure sensors, strain sensors, curvature sensors, and heaters.

In this work, we have developed a sustainable cross-linked poly(castor oil-co-δ-valerolactone)cyclohexyl urethane (PCVU) elastomer for mechanically robust TCE based flexible strain sensors and heaters. PCVU is characterized by its high transmittance (>90%), stretchability (>190%), thermal stability (>210 °C), chemical stability (resistant to various organic solvents), and good degradability in acidic (pH 0, 45% degradation), alkaline (pH 14, 100% degradation), and phosphate buffer (pH 7.2, 9% degradation) aqueous solutions over 150 days, demonstrating its suitability as a sustainable substrate for flexible devices. The flexible and mechanically robust TCE was fabricated using the PCVU, possessing good transmittance

33178 | J. Mater. Chem. A, 2024, 12, 33177–33192

This journal is © The Royal Society of Chemistry 2024

(∼75%) and low sheet resistance (<50 Ω sq^{-1}) at an AgNWs loading of 111.11 μg cm^{-2}. For TCE fabrication, a very thin layer of electrospun PVA was deposited on the PCVU substrate as a temporary wet film leveling agent to improve adhesion and dispersity towards AgNWs, followed by applying heat and pressure-based nano-welding to enhance the conductivity and mechanical stability of the overall TCE. The applicability of the PCVU-based TCE is demonstrated by the fabricating strain sensors and flexible heater. The strain sensor showed good response with low creep in real-time monitoring of human motions (*e.g.*, finger, wrist, elbow and neck movements), and the heater proved effective as a flexible thermotherapy pad.

2. Experimental section

2.1. Materials

All chemicals (castor oil, δ-valerolactone, stannous octoate, and 4,4′-methylenebis(cyclohexyl isocyanate)) and solvents (ethanol and dimethyl formamide) used for the synthesis of the prepolymer and substrate were purchased from Sigma Aldrich and were used as received, without any purification. DMSO-d_6 for NMR analysis was obtained from Merck. PVA (MW = 30 000–70 000 Daltons) and AgNWs (70 nm × 40 μm ($W \times L$)) were also sourced from Sigma Aldrich. The copper tape for the fabrication of the flexible heater and strain sensor was purchased from 3M.

2.2. Instrumentation details

NMR spectra of both the prepolymer and starting materials were obtained with a Bruker 500 MHz spectrometer. Chemical shifts are presented as δ values in ppm, using tetramethylsilane in DMSO-d_6 as the internal standard. FT-IR spectra were recorded on a Bruker FTIR spectrophotometer (VERTEX 70). Thermogravimetric analysis (TGA) and differential thermal analysis (DTA) were performed using a SDT Q600 apparatus from TA Instruments, with a nitrogen flow rate of 100 mL min^{-1} and a heating rate of 10 °C min^{-1}, ranging from 25 °C to 600 °C. Optical transmittance was evaluated from 250 to 1000 nm using a J. A. Woollam VASE ellipsometer. Mechanical properties were assessed through stress–strain tests using a TA.XT.plus100C system from Stable Micro Systems. Surface morphology was analyzed using an Apreo S field-emission Scanning Electron Microscope (SEM) from Thermo Scientific Inc. at 2 kV and 25 pA. Elemental composition was mapped with an EDS attachment (Oxford Instruments UltimMax 100 EDS) connected to the SEM. The texture analyzer (TA.XTplus100C, Stable Micro Systems), equipped with a tensile grip, was used for strain sensor testing under varying conditions. Resistance changes in the strain sensors were measured with an LCR meter (GW-INSTEK LCR-6300) using a 1 V signal at 1 kHz. The sheet resistance of TCEs was measured with an Ossila four-point probe system (Product code: T2001A3), featuring a probe spacing of 1.27 mm. For heating experiments, voltage was supplied by a PeakTech 6225A power supply, and thermal imaging was conducted using a FLIR One Pro infrared camera alongside a FLIR ETS320 integrated with the FLIR Research Studio. The experiments on human subjects were performed after obtaining informed consent.

2.3. Synthesis of prepolymer poly(castor oil-*co*-valerolactone)triol (1)

In a 100 mL round-bottom flask, castor oil (4.9 g, 1 eq., 5.24 mmol), δ-valerolactone (6.46 g, 12.3 eq., 64.57 mmol), and stannous octoate (0.113 g, 1 wt% relative to both monomers) were stirred and allowed to react with each other at 130 °C for 24 hours under a nitrogen atmosphere. Upon completion of the reaction, the catalyst was deactivated by adding 5 mL of methanol to the reaction mixture, followed by stirring for another 10 minutes. Finally, poly(castor oil-*co*-δ-valerolactone)triol was obtained as a viscous liquid after purifying the reaction mixture with hexane (30 mL × 4). This viscous liquid eventually solidified into a white paste after drying in a desiccator at room temperature. The yield of prepolymer was 8.45 g (75%). FTIR: ν_{max}/cm^{-1} 3533–3452 cm^{-1} (ν O–H), 2925–2856 cm^{-1} (ν C–H), 1729 cm^{-1} (ν C=O), 1457–1419–1354 cm^{-1} (δ O–H), 1242–1159 cm^{-1} (ν C–O), 1082–1057–866 cm^{-1} (δ C–H), 721 cm^{-1} (δ C=C). ^{1}H-NMR (500 MHz, DMSO-d_6), δ ppm 5.42–5.28 (m, 6H, castor oil–alkene), 5.18 (s, 1H, castor oil–methine), 4.78 (qu, J = 5.9 Hz, 3H, castor oil–methine), 4.38–4.25 (m, br peak, 4H, castor oil–methylene), 4.00 (s, sharp peak, 6H, valerolactone–methylene), 3.40–3.36 (m, 3H, valerolactone–OH), 2.31–2.23 (m, br peak, 18H, valerolactone–methylene and castor oil–methylene), 1.97 (s, 6H, castor oil–methylene), 1.57–1.24 (m, br peaks, 72H, valerolactone–methylene and castor oil–methylene), 0.85 (s, br peak, 9H, castor oil–methyl). ^{13}C-NMR δ_{ppm} (125 MHz, DMSO-d_6), δ 173.04 (C=O), 132.45, 127.09, 124.86 (C=C), 73.38, 70.24, 69.16 (castor oil–methine), 63.77, 63.68, 60.69 (castor oil–methylene), 36.96, 35.62, 33.93, 3.78, 33.74, 33.50, 33.42, 32.24, 31.94, 31.85, 31.62, 29.88, 29.54, 28.96, 28.01, 27.29, 27.18, 27.07, 25.66, 25.21, 24.92, 24.87, 22.57, 22.47, 21.65, 21.61, 21.48, (castor oil–methylene & valerolactone–methylene), 18.80, 14.28 (castor oil–methyl).

2.4. Synthesis of cross-linked poly(castor oil-*co*-δ-valerolactone)cyclohexyl urethane (PCVU)

The substrate was prepared on a glass mold. In a typical procedure, poly(castor oil-*co*-δ-valerolactone) (1 g, 0.46 mmol, 1 eq.), 4,4′-methylenebis(cyclohexyl isocyanate) (0.24 g, 0.93 mmol, 2 eq.), and stannous octoate (0.043 g, 3.5 wt% relative to both monomers) were dissolved in 1.5 mL of DMF. The solution was drop cast onto a glass mold (150 mm × 150 mm) and subjected to thermal cross-linking polymerization at 75 °C for 3 hours. The resulting substrate, which exhibited high flexibility, transparency, and stretchability, was easily peeled-off from the glass mold as a free-standing film after being cut to the required dimensions.

2.5. Fabrication of flexible and stretchable transparent conducting electrode (TCE)

In a standard procedure, a PCVU substrate (30 mm × 30 mm) was coated with a polyvinyl alcohol (15 wt% in water) nanofabric layer using an electrospinner from Spinbox, applying

This journal is © The Royal Society of Chemistry 2024

J. Mater. Chem. A, 2024, **12**, 33177–33192 | **33179**

a voltage of 22 kV and a flow rate of 2 μL min^{-1}. Subsequently, the PVA-coated substrates were sprayed with silver nanowires (AgNWs) suspended in a 1 : 1 (ethanol : water) mixture at a concentration of 250 μg mL^{-1}. Finally, the substrate was subjected to nano-welding of the AgNW junctions at 120 °C for 20 minutes under an applied pressure of ∼10 kPa. The conductivity and transmittance of the resultant TCE were analyzed using sheet resistance measurements and ellipsometry analysis.

2.6. Degradability studies

The degradability experiments for the PCVU elastomer were conducted under acidic (pH = 1), neutral (PBS; pH = 7.4), and basic (pH = 14) conditions. The studies were carried out at room temperature (RT) by shaking samples on a shaker set at 100 rotations per minute. Each release study was conducted in triplicate. In the standard procedure, substrates measuring 30 mm × 30 mm and weighing approximately 60 mg were placed in 10 mL glass vials. Subsequently, 5 mL of the corresponding pH solutions (pH = 1, pH = 7.4, and pH = 14) were added to each vial and subjected to shaking at RT. At predetermined intervals (1 d, 2 d, 3 d, 8 d, 11 d, 18 d, 28 d, 48 d, 53 d, 72 d, 79 d, 90 d, 110 d, 130 d and 150 d), the release medium was replaced with fresh medium. The weight loss of the substrates in different release media over time was monitored relative to the weight of the corresponding bare substrates.

3. Results and discussion

3.1. Synthesis and characterization of PCVU elastomer

The sustainable PCVU elastomer was synthesized *via* a two-step synthetic approach. Initially, the prepolymer poly(castor oil-*co*-δ-valerolactone)triol was obtained as a viscous liquid by conducting a Ring Opening Polymerization (ROP) between the renewable monomers of castor oil and δ-valerolactone (δ-VL) in the presence of Sn(II) octoate catalyst under N$_2$ at 130 °C for 24 h without a solvent. These monomers were selected for the prepolymer synthesis because of their biodegradability and nontoxic properties.[51,52] The ester linkage (–(C=O)–O–) in the prepolymer enables it to undergo hydrolytic degradation. Therefore, the developed prepolymer is an environmentally responsible choice for the preparation of degradable elastomeric substrate. Additionally, the prepolymer with terminal hydroxyl groups is suitable for chemical modification to accomplish an elastomer with suitable mechanical properties. Hence, in the second step, the prepolymer was reacted with 4,4′-methylenebis(cyclohexyl isocyanate) (HMDI) in 1 : 2 molar ratio in the presence of dimethyl formamide (DMF) and Sn(II) octoate at 75 °C for 3 h to yield PCVU elastomer (Fig. 1a). This step was carried on a glass mold, whereas the reaction mixture was dropcast and thermally baked to prepare cross-link PCVU elastomer in the form of peelable and free-standing films. The prepolymer and HMDI were used to compose soft and hard segments combinations in the PCVU elastomer respectively as shown in Fig. 1a. Hard segments can contribute mechanical properties such as hardness and toughness to PCVU elastomers, while soft

segments can enhance degradability, flexibility, stretchability, and increase the mobility of the polymeric chains within the elastomer.

By maintaining the prepolymer and HMDI in 1 : 2 molar reactivity ratios, we obtained the PCVU elastomer that demonstrates high transmittance, and skin-like multifunctional properties including relaxing, stretching, twisting, bending, and conformal skin attachment, as shown in Fig. 1b. However, we noticed that the change of HMDI concentration during PCVU synthesis affects the homogeneity between soft and hard segments, impacting physicochemical properties of the elastomer. Reducing the HMDI to 1 or 0.5 molar ratios results in films that cannot be peeled, likely due to an insufficient mix of hard and soft segments for effective cross-linking. On the other hand, increasing the HMDI to 3 molar ratios causes the PCVU elastomers to exhibit almost no transmittance (Fig. S1, ESI†). Noticing a lack of homogeneity due to thermodynamic noncompatibility between the soft and hard segments is quite a common phenomenon for polyurethane elastomers.[53] Generally, this challenge can be addressed by adjusting the combinations and proportions of hard and soft segments, controlling the length of soft segments, cross-linking density, and other factors.

To characterize the functional groups in a prepolymer and PCVU elastomer by comparing them with starting monomers (castor oil, δ-VL, and HMDI), Fourier Transform Infrared Spectroscopy (FT-IR) was employed and the spectra is shown in Fig. 2a and b. Castor oil displayed IR peaks at 3401, 2921, and 1742 cm^{-1}, attributed to the stretching vibrations of O–H, C–H, and C=O groups, respectively. δ-VL and HMDI exhibited IR bands at 1735 cm^{-1} and 2246 cm^{-1}, corresponding to stretching vibrations associated with cyclic ester (–(C=O)–O–) and isocyanate (–N=C=O) groups, respectively. The prepolymer displayed a C=O stretching frequency at 1725 cm^{-1}, which was lower than that in δ-VL (1735 cm^{-1}), suggesting the formation of the prepolymer from a ROP of δ-VL with castor oil. Additionally, the O–H groups in the prepolymer showed a higher stretching frequency at 3538 cm^{-1} compared to those in castor oil (3401 cm^{-1}), further confirming the formation of the prepolymer. PCVU did not show any IR band for –N=C=O at 2246 cm^{-1} and displayed stretching frequencies for N–H and C=O groups for urethane and ester linkages at 3368 and 1731 cm^{-1} respectively, confirming a cross-linking polyurethane reaction between the prepolymer and HMDI. For PCVU elastomer, the N–H peak is shifted to a lower wavenumber and the C=O peak to a higher wavenumber compared to the O–H and C=O group frequencies in the prepolymer, clearly suggesting the existence of a urethane (–NH–(C=O)–O–) linkage. Furthermore, the dense C–H functionality in the polymer backbone of both the prepolymer and PCVU elastomer was confirmed by observing stretching frequencies at 2922 cm^{-1} and 2925 cm^{-1}, respectively.

Further, Nuclear Magnetic Resonance (NMR) analysis was performed to characterize the prepolymer in comparison to its starting monomers. The assignment of proton NMR peaks for castor oil, δ-VL, and the prepolymer according to their chemical structures is shown in Fig. 2c. The prepolymer confirmed with

33180 | *J. Mater. Chem. A*, 2024, **12**, 33177–33192

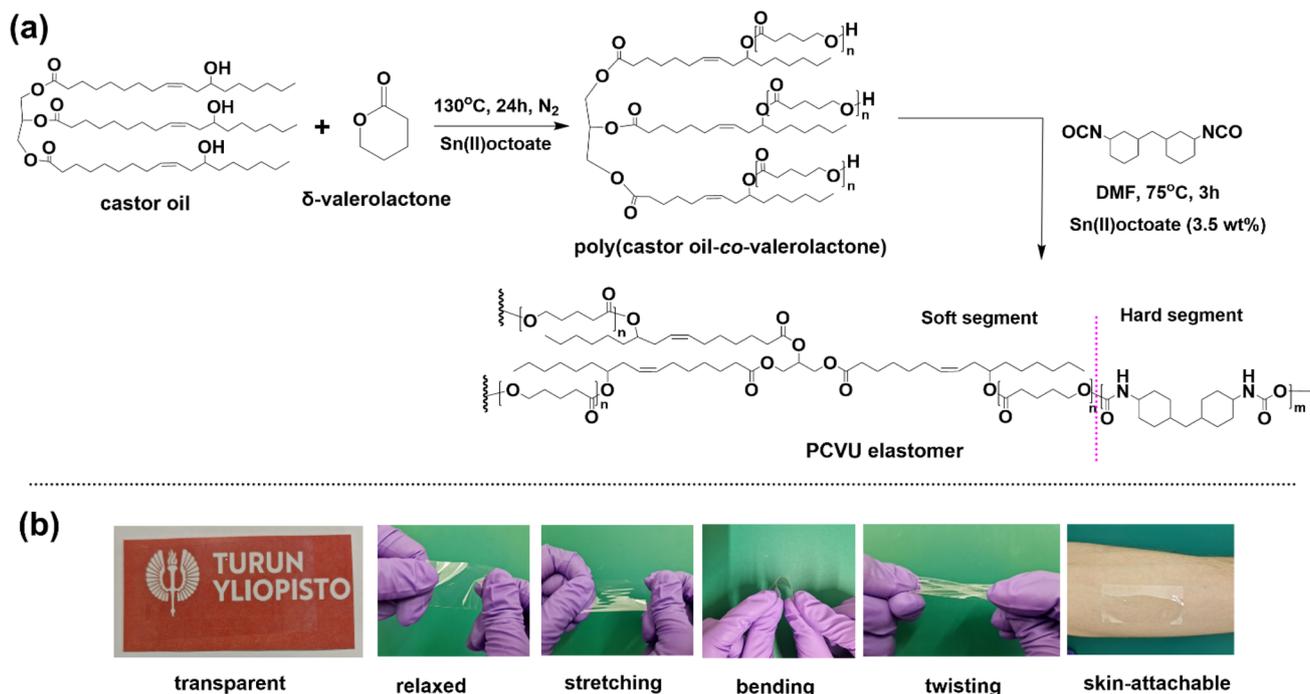This journal is © The Royal Society of Chemistry 2024

Fig. 1 (a) Synthetic route for PCVU elastomer. (b) Photographs of the PCVU elastomer displaying its transparency with the University of Turku logo visible underneath, and demonstrating various physical states including relaxed, stretched, bent, twisted, and conformally attached to human skin.

a stable tri-ester structure for the castor oil segment by displaying characteristic methine and methylene protons (a and e) at 5.18 ppm and 4.35–4.25 ppm, respectively. Additionally, it showed chemical shifts for alkene protons (b and c) in the deshielding region at 5.40–5.30 ppm, due to the presence of the castor oil unit in the prepolymer backbone. The methine proton (d) of castor oil in the prepolymer shifted to the deshielding region at 4.77 ppm, compared to 4.34 ppm in free castor oil, confirming the occurrence of ROP between castor oil and δ-VL. The methylene repeating (f) and terminal (g) protons of VL chains in the prepolymer were observed at 4.00 ppm and 3.38 ppm, respectively, which are not present in the starting monomers (both castor oil and δ-VL), further confirming the formation of the prepolymer. Additionally, a sharp resonance peak at 1.56 ppm was attributed to the dense methylene functionality (p and q) of VL chains in the prepolymer. The formation of the prepolymer was also supported by similar poly(glycerol-co-caprolactone)triol structures reported in the literature.[54] Based on the integration difference between (f) and (g) protons, the number of repeating VL units (n) and the number-average molecular weight (M_n) of the prepolymer have been calculated as 6.6 and 2933.45 g mol^{-1}, respectively. However, due to the insoluble characteristics of the PCVU elastomer in organic solvents, NMR studies were not conducted for this material.

To understand thermal properties such as glass transition temperature (T_g), melting temperature (T_m), and thermal stability of the prepolymer and PCVU elastomer, we subjected them to thermogravimetric analysis (TGA) and differential scanning calorimetry (DSC) analysis (Fig. 2d and e). The prepolymer displayed a T_m in the DSC at 23.60 °C, confirming its crystalline nature. In contrast, the PCVU did not display any T_m and showed only a T_g at −47.8 °C, indicating the amorphous nature of the PCVU due to its crosslinked network structures. TGA analysis showed that the PCVU elastomer was thermally stable until 210 °C, compared to the prepolymer, which was thermally stable only until 100 °C. The improved thermal stability observed in the PCVU can be attributed to its stable crosslinked ester–urethane network structures, in contrast to the non-crosslinked prepolymer. However, both the prepolymer and PCVU elastomer begin losing mass beyond their thermally stable temperatures, eventually exhibiting 100% mass loss at 450 °C in both cases.

To study optical properties of the PCVU elastomer (thickness 150 μm, 3 cm × 3 cm film), we subjected it to transmittance studies in the wavelength range of 400–800 nm. The PCVU displayed excellent transmittance, nearly 90% (Fig. 3a), highlighting its potential for transparent electronics applications. This level of transmittance is comparable to that of highly transparent plastic substrates such as polyethylene terephthalate (PET),[55] polyimide (PI),[56] polycarbonate (PCs),[57] as well as elastomeric substrates like PDMS,[58] TPU,[59] and synthetic biodegradable poly(L-lactide-co-ε-caprolactone) (PLCL)[60] substrates, all of which exhibit around 90% transmittance at similar thickness levels reported in the literature. Additionally, PCVU surpasses other commercial elastomer film Ecoflex (~72%),[61] and plastic substrate polyethylene naphthalate (PEN) (~80%)[62] when compared at similar thicknesses.

To investigate the mechanical properties of the PCVU elastomer, we subjected it to a mechanical testing for stress–strain
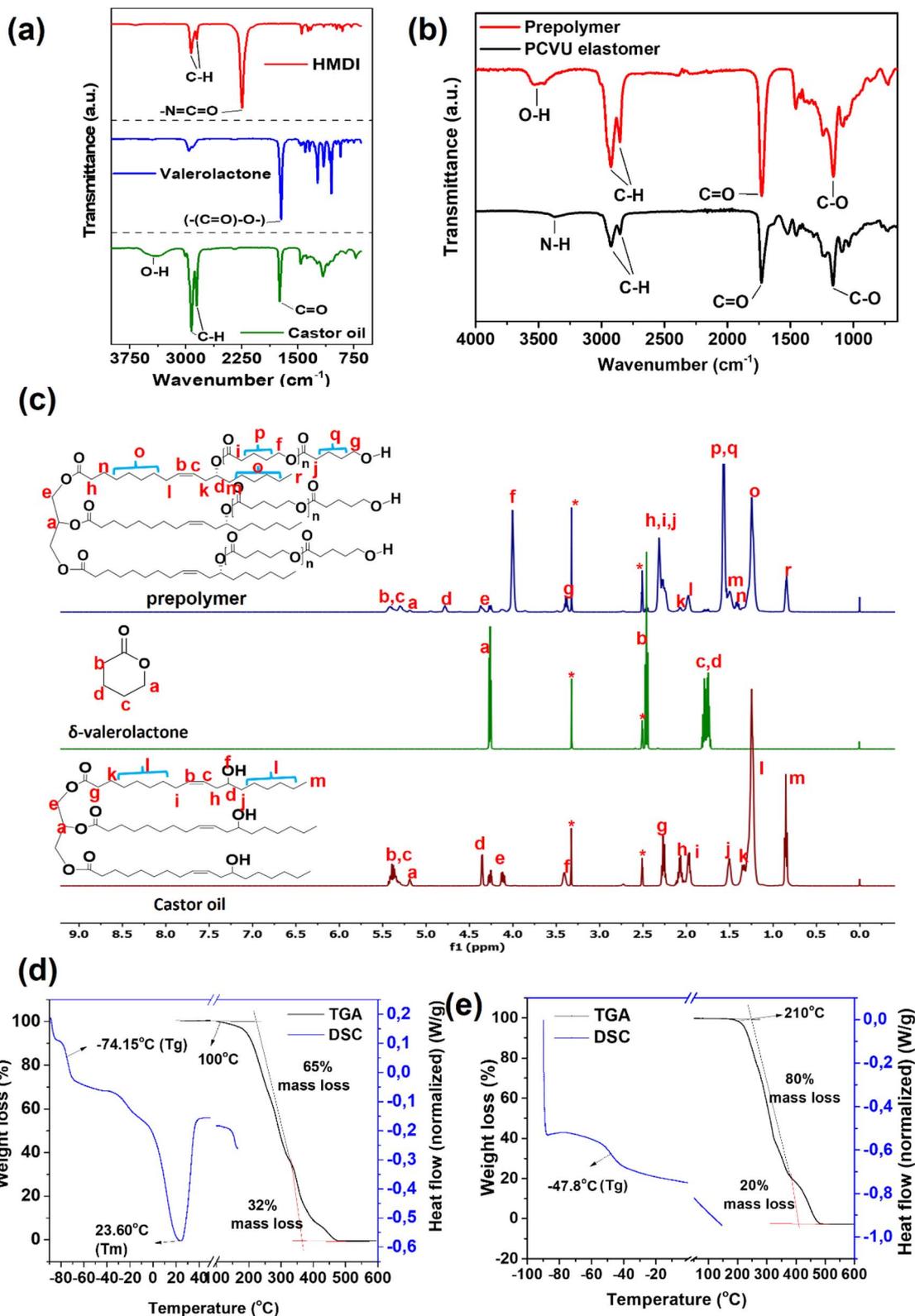
This journal is © The Royal Society of Chemistry 2024

J. Mater. Chem. A, 2024, **12**, 33177–33192 | **33181**

Fig. 2 (a) FT-IR profiles of starting monomers castor oil, δ-VL, and HMDI. (b) FT-IR profiles of prepolymer and PCVU elastomer. (c) ¹H-NMR profile of prepolymer with the comparison of starting monomers castor oil and δ-VL. (d) TGA and DSC profiles of prepolymer and (e) PCVU elastomer.
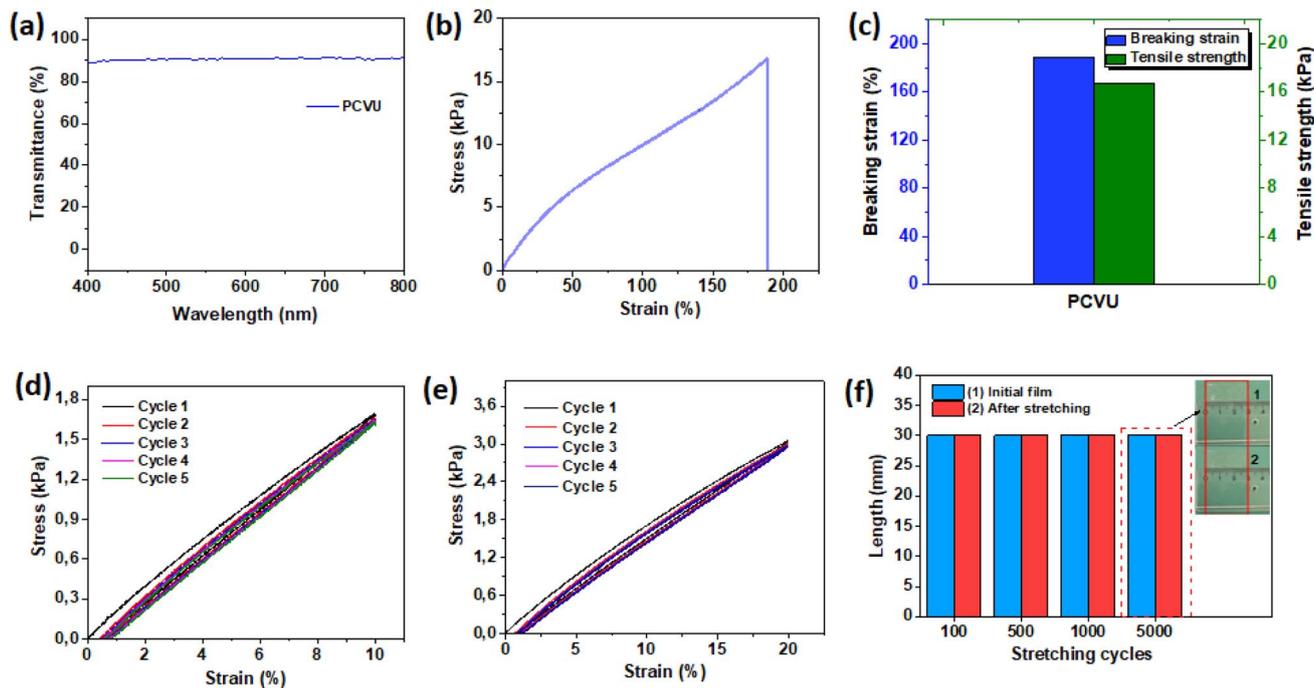
33182 | J. Mater. Chem. A, 2024, 12, 33177–33192

This journal is © The Royal Society of Chemistry 2024

Fig. 3 Characterization data of PCVU elastomeric substrate (a) transmission data, (b) stress *vs.* strain profile, (c) tensile strength and breaking strain of PCVU substrate, (d) cyclic strain *vs.* stress profile at 10% strain, and (e) 20% strain. (f) State recovery of PCVU elastomer after undergoing multiple stress–strain over 100, 500, 1000 and 5000 cycles at 20% of strain.

analysis. The PCVU exhibited a breaking strain of 190% under a tensile strength of 16.75 kPa, confirming its elastic properties (Fig. 3b and c). Furthermore, to compare the mechanical properties of our PCVU elastomer with those of human forearm skin, we calculated the modulus of elasticity, or Young's modulus (E), from its stress–strain curve (Fig. S2, ESI†). Like skin and other biological tissues, the stress–strain profile of our PCVU elastomer showed typical nonlinear behavior.[63] The modulus of elasticity is theoretically derived from the slope of a linear stress–strain curve. However, for a typical nonlinear stress–strain curve, calculating the slope is not feasible due to its non-linear characteristics.[63,64] In the literature, the modulus of elasticity for skin-like elastomers that exhibit nonlinear stress–strain characteristics is determined by calculating the slope at the E_1 and E_2 regions, which correspond to the initial extension of the sample under low strain conditions and the linear region of the curve with the highest strain conditions, respectively.[64] Based on this, the calculated elastic moduli of our PCVU elastomer at E_1 and E_2 are ~0.14 kPa and ~0.09 kPa, respectively. These values closely align with Young's modulus of the human forearm epidermis and soft tissues such as the spleen, liver, pancreas, and adipose tissue, which range from 0.1 to 10 kPa.[63,65] This comparison suggests that the mechanical properties of the PCVU elastomer closely mimic those of human skin, highlighting its suitability for electronic skin (e-skin) and flexible device applications.

Resilience is crucial for elastomers aimed at stretchable and flexible devices. Thus, to assess the stretching and recovery characteristics, we subjected the PCVU elastomer to cyclic stress–strain tests under different applied strain conditions. Fig. 3d and

e show the stress–strain profiles of the PCVU elastomer, subjected to strains of 10% and 20% over five cycles, respectively. The results demonstrated that the PCVU elastomer exhibited rapid expansion and quick recovery due to low or negligible hysteresis. However, the slight shift observed in the first cycles of Fig. 3d and e at 10% and 20% strain might be due to the settling of the polymer films on the texture analyzer during initial stages. The settling of stretchable films when first subjected to mechanical testing is commonly seen in the case of polyurethane films.[66,67] After the first round of stress–strain cycles, the hysteresis returned to its original position within 2 to 5 cycles, indicating negligible hysteresis and complete elastic recovery of the film. This property is crucial for applications in flexible sensors and actuators, including artificial muscles, skin-like sensors, and interfaces between electronics and biological tissues.[68] Owing to its negligible hysteresis, our PCVU substrate exhibited no shape deformation even after 100, 500, 1000 and 5000 stress–strain cycles at 20% strain (Fig. 3f). After the cyclic studies, the PCVU elastomer returned to its original length upon strain release, demonstrating complete recovery (inset, Fig. 3f). This resilience underlines the PCVU substrate's potential for practical applications in flexible and stretchable devices.

3.2. Chemical resistance and degradability studies of PCVU elastomer

Understanding the chemical resistance and swelling behavior of substrates when exposed to different solvents is crucial for their use in the fabrication of TCE and flexible devices. Typically, the TCE fabrication process involves exposing substrates

to various chemicals and conductive materials dissolved in solvents. An ideal substrate for fabricating highly durable TCEs should exhibit high chemical stability and no swelling. As previously discussed, most available traditional silicon-based elastomers (*e.g.*, PDMS, Ecoflex, Sylgard, dragon skin, *etc.*) demonstrate poor solvent resistance due to swelling,[69,70] which affects device fabrication and stability. Thus, it is essential to understand the chemical stability of a newly developed substrate.

To study the swelling behavior and dissolution properties of the PCVU elastomer, we exposed it to various organic solvents such as methanol, ethanol, isopropanol, dimethylformamide, and dichloromethane over different time intervals (1 h, 2 h, 5 h, 19 h, and 24 h) at room temperature (RT). The weight of PCVU substrates in different solvents over time in comparison to their initial weights (before solvent exposure) was shown in Fig. 4a and Table S1 (ESI†). Studies demonstrate that PCVU did not show any weight changes or dissolution behavior over time in different solvents. The relevant morphological images of PCVU exposed to different times in comparison to the bare starting film (without solvent exposure) were shown in Fig. S3 (ESI†), indicating that the elastomer maintained its original physical state with no solvent absorption or dissolution. These studies highlight the potential chemical stability of PCVU elastomers for use in the TCE fabrication process.

Furthermore, to study the degradability properties of our PCVU substrate, we exposed it to acidic (pH = 0), neutral (PBS, pH = 7.4), and basic (pH = 14) aqueous solutions, and monitored its degradation rate over 150 days at room temperature (Fig. 4b). Details of the degradation procedure are provided in the experimental section. The PCVU fully degraded (100%) in the basic medium within 72 days, while it showed 45% and 9% degradation in acidic and PBS solutions over 150 days respectively. The faster degradation of PCVU films in acidic and basic media is likely due to accelerated ester bond cleavage by OH^- and H^+ ions.[42,71,72] A possible mechanism for base-mediated ester bond cleavage in PCVU is shown in Fig. S4, ESI.† The hydrolytic degradation of PCVU films in PBS (pH = 7.2), which is within the pH range of tap water (6.5–8.5)[73] and biological media (pH 7.2), indicates that PCVU films can degrade under standard conditions. Additionally, the synthesis of PCVU is mainly based on the biocompatible prepolymer "poly(castor oil-*co*-δ-valerolactone)triol," which is synthesized from renewable non-toxic monomers such as castor oil and valerolactone. Therefore, the degraded products from the PCVU elastomer could potentially be non-toxic and environmentally friendly, which can include fatty acids, hydroxyvaleric acid, glycerides, *etc.* (Fig. S4, ESI†). This demonstrates PCVU is a sustainable and environmentally compatible material, making it an excellent choice for sustainable flexible devices.

3.3. Fabrication and characterization of transparent conducting electrode (TCE)

The flexible TCE was fabricated using PCVU (30 mm × 30 mm) as a substrate. The essential properties of the PCVU include high transmittance, resistance to deformation under high strain conditions, high thermal stability, and skin-like multi-functional properties, making it suitable for TCE fabrication. The fabrication process of TCE was shown in Fig. 5.

Applying a wet film leveling agent to the substrate surface is important for controlling surface irregularities and enhancing surface area during electrode fabrication. The leveling agent can helps in uniform spreading of conductive nanomaterials during their deposition on the substrate surface. For sustainable TCE fabrication, we considered applying a very thin layer of electrospun polyvinyl alcohol (PVA) as a temporary wet film leveling agent on the PCVU surface. PVA is a water-soluble, nontoxic, and environmentally friendly polymer. The hydrophilic electrospun PVA network can enhance the surface area of the PCVU, allowing the conductive nanowires spray-coated during the fabrication process to spread uniformly across the substrate surface. Therefore, in the first step of the TCE fabrication process, we used the electrospinning technique to deposit a very thin layer of PVA across the PCVU substrate surface (please refer to the experimental section for PVA electrospinning details). SEM analysis confirmed the presence of a very thin PVA nano-fabric mat distributed across the PCVU with an average nano-fiber diameter of ~80 nm (Fig. 6a). The nanofiber mat was randomly oriented, which helps in the uniform spreading of AgNWs across the PCVU due to increased surface area.
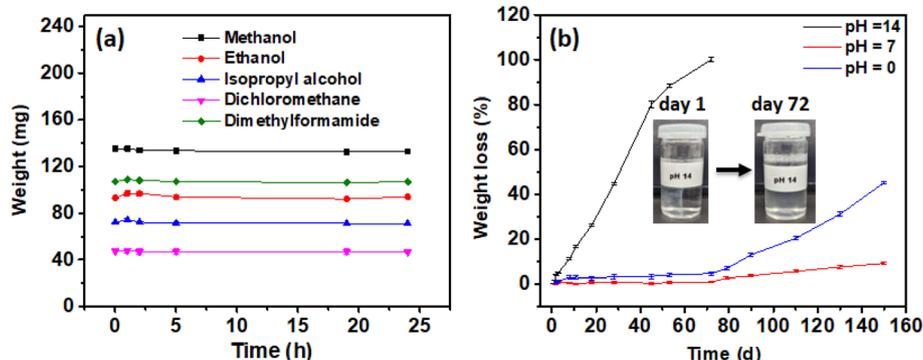

Fig. 4 (a) Chemical stability profile of PCVU exposed in different organic solvents over time, (b) degradation profile of PCVU elastomer over time in different pH aqueous solutions at pH = 0, pH = 7 and pH = 14.
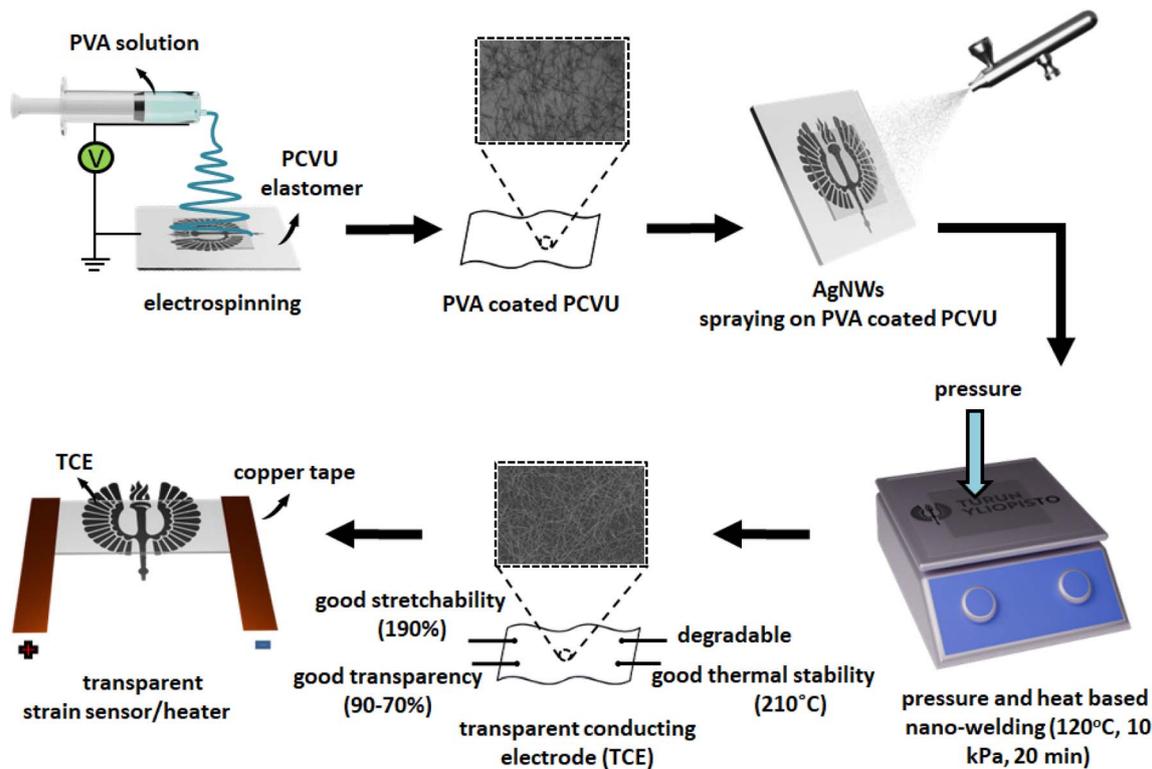
33184 | *J. Mater. Chem. A*, 2024, **12**, 33177–33192

This journal is © The Royal Society of Chemistry 2024

Fig. 5 Fabrication of PCVU based TCE and its flexible heater.

Subsequently, in the second stage, AgNWs (aspect ratios 70 nm × 40 μm) dispersed in ethanol : water (1 : 1 ratio) at an optimized concentration of 250 μg mL^{-1} were sprayed onto the PVA-coated PCVU for uniform spreading. We studied the spreading mechanism of AgNWs solution on the PVA-coated PCVU in comparison to PCVU alone as a reference (Fig. S5, ESI†). When sprayed, the AgNWs solution exhibited uniform and rapid spreading on the PVA-coated PCVU. In contrast, the control surface (PCVU alone), which lacks the PVA coating, displays no spreading of the AgNWs solution (refer Fig. S5, ESI†). This difference can be explained based on the capillary

and viscous frictional forces.[74] During spraying, AgNWs are delivered as numerous small droplets that quickly spread upon touching the PVA nanofabric surface, due to capillary and viscous frictional forces (Fig. S5c, ESI†). This spreading is facilitated by the high surface area of the PVA nanofibers, which increases the pressure gradient. The PVA nanofabric layer likely enhances capillary forces, causing the AgNWs droplets to spread outward, while viscous friction forces resist this movement. The spreading of AgNWs droplets on the substrate surface depends on the balance between these two forces. However, friction forces become less significant on PVA-coated
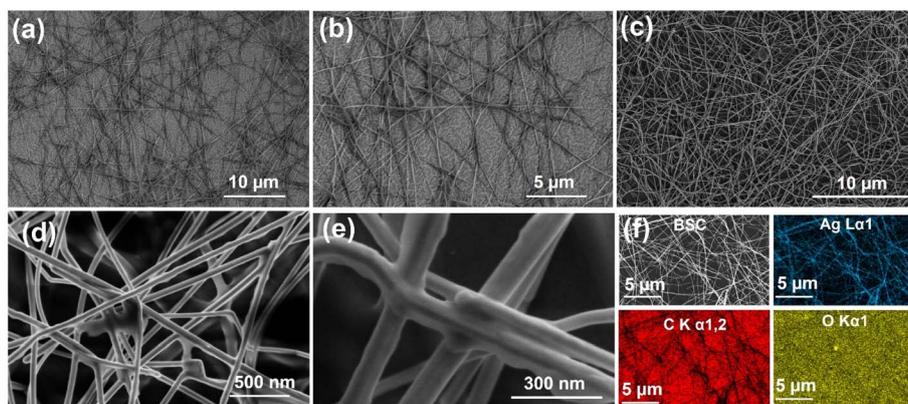

Fig. 6 SEM characterization of TCE. (a and b) Electro spun PVA nano fabric network on PCVU substrate. (c) AgNWs distributed across the TCE. (d and e) High resolution SEM images showing the nano welded of AgNWs junctions on the TCE. (f) Back scattered electrons for AgNWs network across TCE and corresponding EDS for silver, carbon, and oxygen elements.

PCVU surfaces compared to bare PCVU surfaces. The hydrophilic nature of PVA nanofibers on the PCVU promotes strong interactions with the ethanol : water droplets, thus reducing the resistance to droplet movement compared to the base PCVU substrate (Fig. S5c, ESI†). These experiments support our claim that the PVA nanofabric layer acts as an effective wet film leveling agent, facilitating the uniform spreading of AgNWs in the ethanol : water mixture across the substrate surface.

It is worth mentioning that the PVA layer acts as a temporary leveling agent, as it disappears after spraying silver nanowires on the PCVU surface. The disappearance of the PVA mat on the TCE surface is clearly visible in Fig. S5b, ESI.† Therefore, the PVA fabric mat applied to the PCVU surface is only intended to promote the uniform spreading of AgNWs across the PCVU and has no significant role in improving the TCE properties. PCVU offers high transmittance, stretchability, flexibility, and thermal stability to TCE, while the AgNWs provide outstanding conductive properties. Therefore, PCVU is a potentially suitable choice for making flexible devices for heater and strain-sensing applications, and the PVA layer had no role in this.

To enhance the performance of TCEs, it is crucial to minimize the resistance at the junctions of AgNWs and usually done using different nanowelding techniques.[22] This approach significantly boosts the TCE's electrical conductivity with enhanced mechanical stability, and durability. In the third step, the AgNWs on the PCVU film were subjected to nano-welding to minimize the junction resistance. This process was conducted on a hot plate, where the AgNWs sprayed PCVU films were subjected to heat and pressure-based nano-welding at 120 °C and a pressure of 10 kPa for 15 minutes. SEM analysis confirms the uniform spreading of

AgNWs along with the nano welded structures across the PCVU. Fig. 6c and d showed densely packed AgNWs those randomly oriented atop each other on the PCVU surface. The high-resolution SEM analysis showed that the nano welded AgNWs structures with an average diameter of ∼70 nm as displayed in Fig. 6e. Due to the welded AgNWs network, TCE showed improved and uniform electrical properties with low sheet resistance characteristics in comparison to TCE that was not subjected for nano welding. The measured resistance of TCE (AgNWs loading is 111.11 μg cm^{-2}) before nano-welding exhibited non-uniform and high values ∼300 Ω sq^{-1}, which is significantly drops to ∼50 Ω sq^{-1} after nano welding. This study confirms the importance of nano welding approach. Furthermore, Energy-Dispersive X-ray Spectroscopy (EDS) analysis confirms the uniform distribution of AgNWs across the PCVU films. The EDS mapping profiles for the elements silver (Ag), carbon (C), and oxygen (O) are shown in Fig. 6f.

The effect on the optical and electrical properties of TCE by varying AgNWs loading (44.44, 66.66, 88.88, 111.11, and 133.33 μg cm^{-2}) was studied. This study is crucial for optimizing the electrical and transmittance properties of the TCE. The transmittance and sheet resistance of TCEs are inversely proportional to the AgNWs loading density, especially when coated on planar substrates. However, there are some methods and three-dimensional substrates where the nanowires can be deposited in unique patterns to maintain the transmittance.[27,49] Fig. 7a shows the decrease in TCEs' transmittance with the increase in AgNW density from 44.44 to 133.33 μg cm^{-2}. The trend in the reduction of transmittance is attributed to the strong scattering and reflection of photons at higher AgNW densities.[75] However,
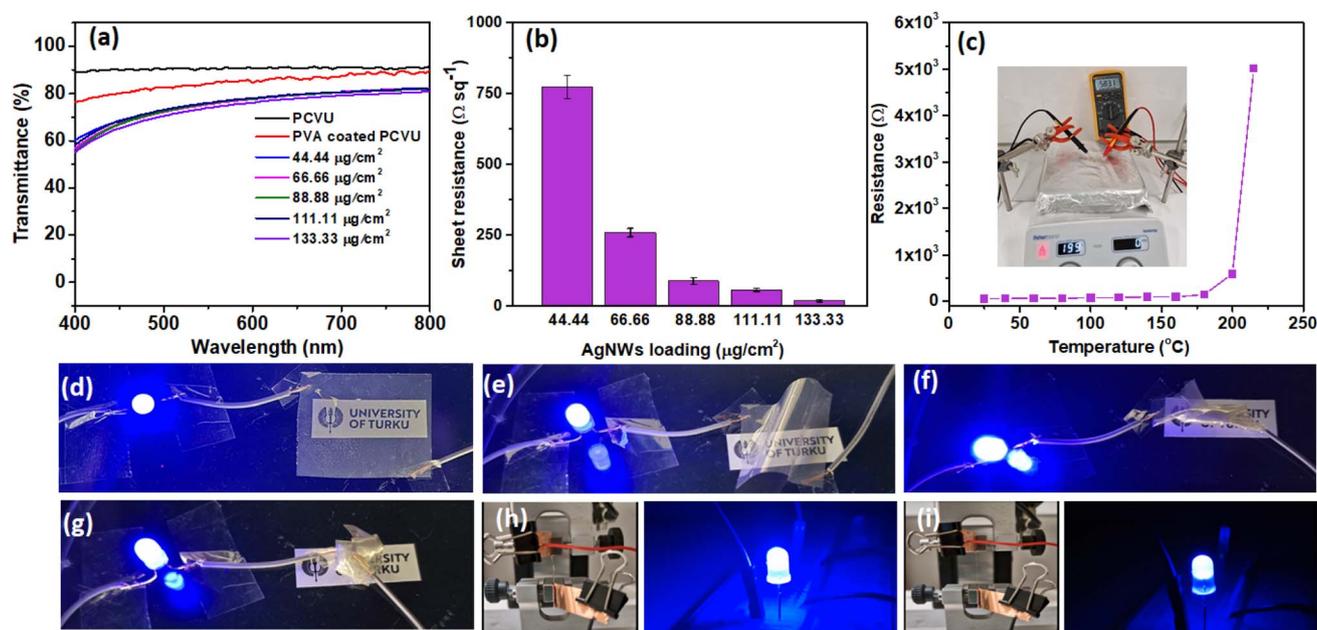

Fig. 7 (a) Transmittance data of PCVU elastomer loaded with different AgNWs loading (44.44, 66.66, 88.88, 111.11, 133.33 μg cm^{-2}). (b) Sheet resistance effect on increasing AgNWs loading. (c) Resistance vs. temperature profile of PCVU based TCE. Testing flexible properties of TCE connecting as a conductor in a circuit to power an LED: TCE showing high-intensity LED brightness in (d) normal, (e) bending, (f) twisting, and (g) crumpled conditions. TCE shows reversible change in brightness of LED under (h) relaxed and (i) stretched conditions.

33186 | J. Mater. Chem. A, 2024, 12, 33177–33192

This journal is © The Royal Society of Chemistry 2024

TCEs with a high density of AgNWs still display decent optical transmittances. For example, TCEs with AgNW densities of 111.11 and 133.33 µg cm^{-2} showed transmittances of approximately ~75% and ~70%, respectively. These values are significantly lower than the base PCVU transmittance (90%) but are relatively comparable with the transmittance (80%) of commercial ITO deposited on PET.[76] These findings suggest that our PCVU-based TCEs can maintain good transparency even at high AgNW loading densities, representing their potential use in transparent electronic devices. On the other hand, the sheet resistance of TCEs also decreases as the AgNW loading increases from 44.44 to 133.33 µg cm^{-2} (Fig. 7b). Increasing the AgNW density on the TCE enhances the conductive network by forming more junctions for electron transfer, thus a decrease in the sheet resistance of the TCEs is observed. These findings are helpful for tailoring the electrical properties of TCEs mainly by adjusting the AgNW loading.

Furthermore, the stability of AgNWs on the TCE and their relationship with resistance change as the temperature increases were studied. These studies are crucial, especially when the TCE is used for flexible heater applications. A constant rise in temperature (20 °C per 10 min) was applied to the TCE (AgNWs loading of 111.11 µg cm^{-2} and sheet resistance of ~50 Ω sq^{-1}) on a hot plate from 25 °C to 215 °C and their corresponding changes in the resistance were recorded using a multimeter. Fig. 7c showed that the resistance of the TCE remained stable up to ~160 °C and beyond that there was a notable increase in the resistance was noticed. This is likely due to heat-induced degradation or breaking of the AgNWs junctions on the

TCE, which increase the resistance of the TCE.[77] These results highlight that the fabricated TCE can maintain reliable conductivity up to at least 160 °C, making it suitable for use in high-temperature-resistant flexible electronics.

To study the electrical performance of PCVU-based TCE under various mechanical deformations, we tested TCE as a conductor in a circuit to light an LED and examined its performance under conditions such as normal, bending, twisting, crumpling, relaxing, and stretching at 2 V (Fig. 7d–i). The conductivity of the TCE remained stable, with no visible change in the LED brightness during normal, bending, twisting, crumpling, and relaxing conditions (Fig. 7d–h). In contrast, when the TCE was stretched with an applied strain of 20%, a noticeable decrease in the LED brightness was observed (Fig. 7i). This decrease in conductivity or increase resistance is due to the AgNWs becoming more oriented along the direction of the applied strain, leading to fewer contact points for conductivity between the AgNWs. However, once the strain is released, the conductivity of the TCE returns to its original state (decrease resistance) due to the reorientation of the AgNWs, which increases the number of contact points, which results in higher LED intensity (please see Video S1, ESI files†). This can be due to the high aspect ratio (70 nm × 40 µm; width × length) of the AgNWs used in the TCE fabrication process. These nanowires are randomly oriented and nano-welded at junctions (see Fig. 6c–e), allowing the TCE to maintain conductivity during stretch–release cycles. These studies demonstrate that our TCE is flexible and durable, maintaining its conductivity under various mechanical deformations. It exhibits a reversible
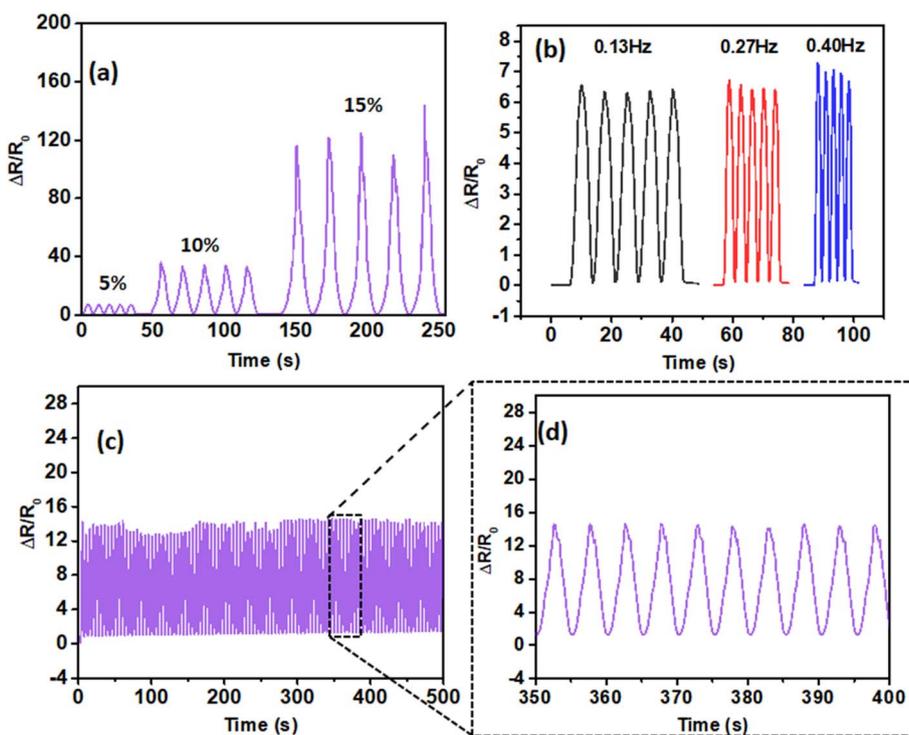

Fig. 8 Strain sensor data. (a) Sensor shows an increase in resistance with increasing strain from 5% to 15%. (b) Sensor demonstrates stable sensing under various applied frequencies (0.13 Hz, 0.27 Hz, and 0.40 Hz) at 5% applied strain. (c) Stretching−releasing cyclic data of the sensor tested at 5% applied strain over 100 cycles. (d) Zoomed view from (c) showing stable resistance change of the TCE.

change in conductivity during stretching and releasing, underscoring its suitability for flexible and stretchable electronic device applications.

3.4. Strain sensor fabrication and testing

The applicability of the TCE was evaluated by fabricating and testing it as a strain sensor (30 mm × 12 mm dimension). The change in resistance ($\Delta R/R_0$) of the sensor as a function of increasing strain was measured using an LCR meter combined with a texture analyzer. Fig. 8a shows that the sensor based on PCVU can withstand strains up to 15% while exhibiting a stable $\Delta R/R_0$ response. However, beyond 15% strain, the sensor displayed inconsistency in $\Delta R/R_0$. This instability is likely due to crack-induced failure of the AgNWs on the TCE.[78] The sensor demonstrated consistent sensing performance by maintaining a stable $\Delta R/R_0$ change across various stretching frequencies (0.13 Hz, 0.27 Hz, and 0.40 Hz) at an applied strain of 5% (Fig. 8b), indicating that the performance of the sensor is frequency independent. Additionally, the durability of the strain sensor was tested by subjecting it to 100 stretching–releasing cycles at 5% strain, during which it showed stable $\Delta R/R_0$ changes, indicating its reliable performance and long-term stability (Fig. 8c and d).

As the strain sensor displays stable and repeatable $\Delta R/R_0$ changes under various applied strain conditions, we have demonstrated its utility for real-time motion monitoring applications. The sensor was tested for monitoring a variety of human body motions, including finger joint, wrist, elbow, and neck movements. The sensor was able to distinguish these movements effectively. As shown in Fig. 9a, the strain sensor mounted on the finger joint displayed stable and repeatable $\Delta R/R_0$ changes in response to bending–releasing activities. Additionally, a periodic change in $\Delta R/R_0$ was observed when the strain sensor mounted on the wrist and elbow underwent similar bending–releasing activities, as illustrated in Fig. 9b and c. Finally, the strain sensor attached to the throat also showed distinguishable $\Delta R/R_0$ changes for neck extension and flexion cycles (Fig. 9d). These studies highlight good sensitivity, repeatability, and selectivity of the sensor for real-time human motion monitoring, making it a promising candidate for wearable health monitoring devices.

3.5. Flexible transparent heater fabrication and testing

The Joules heating characteristics of the PCVU-based TCE were studied by fabricating a flexible transparent heater. Transparent heaters are broadly applied across many technologies to deliver essential warmth, including avionics, microfluidic chips, automative windows, defogging mirrors, smart clothing, and thermotherapy patches.[79] To fabricate the heater, a stretchable TCE (30 mm × 20 mm) with a uniform sheet resistance of ~50 Ω sq^{-1} and transparency of ~75% was utilized by connecting it on either side with copper tapes (Fig. 4). Thermal analysis was done using FLIR thermal studio, measuring data at the nonconductive surface area.

To investigate the steady-state saturation temperature (T_s) and heating characteristics, a continuous DC voltage ranging
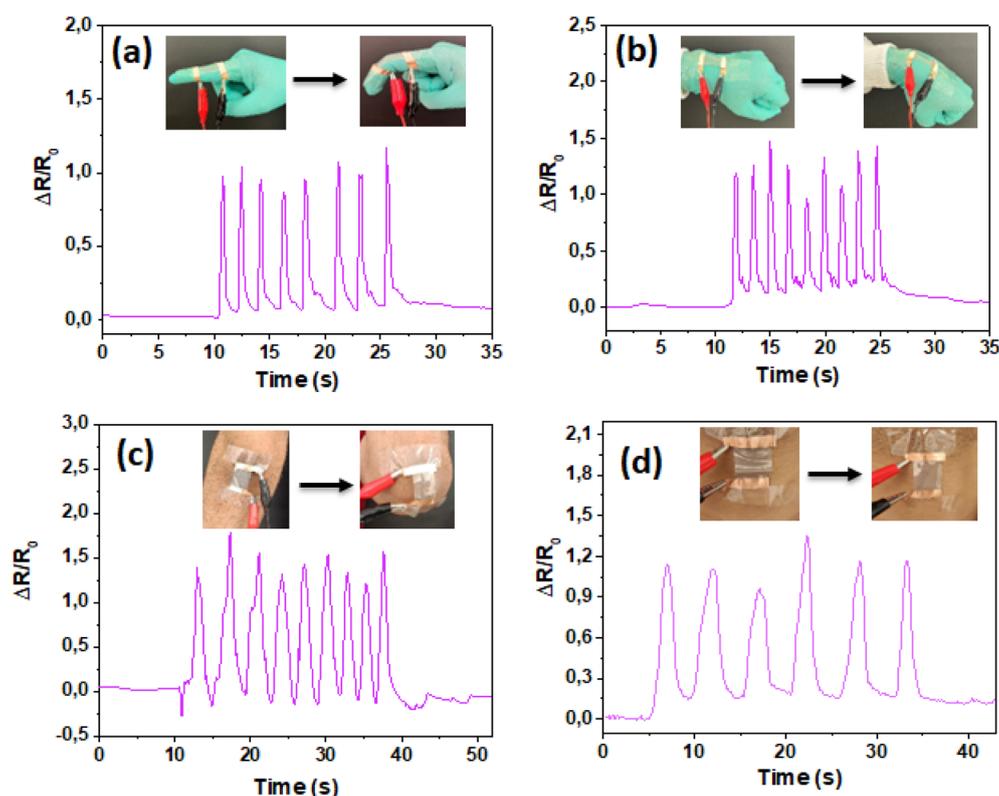

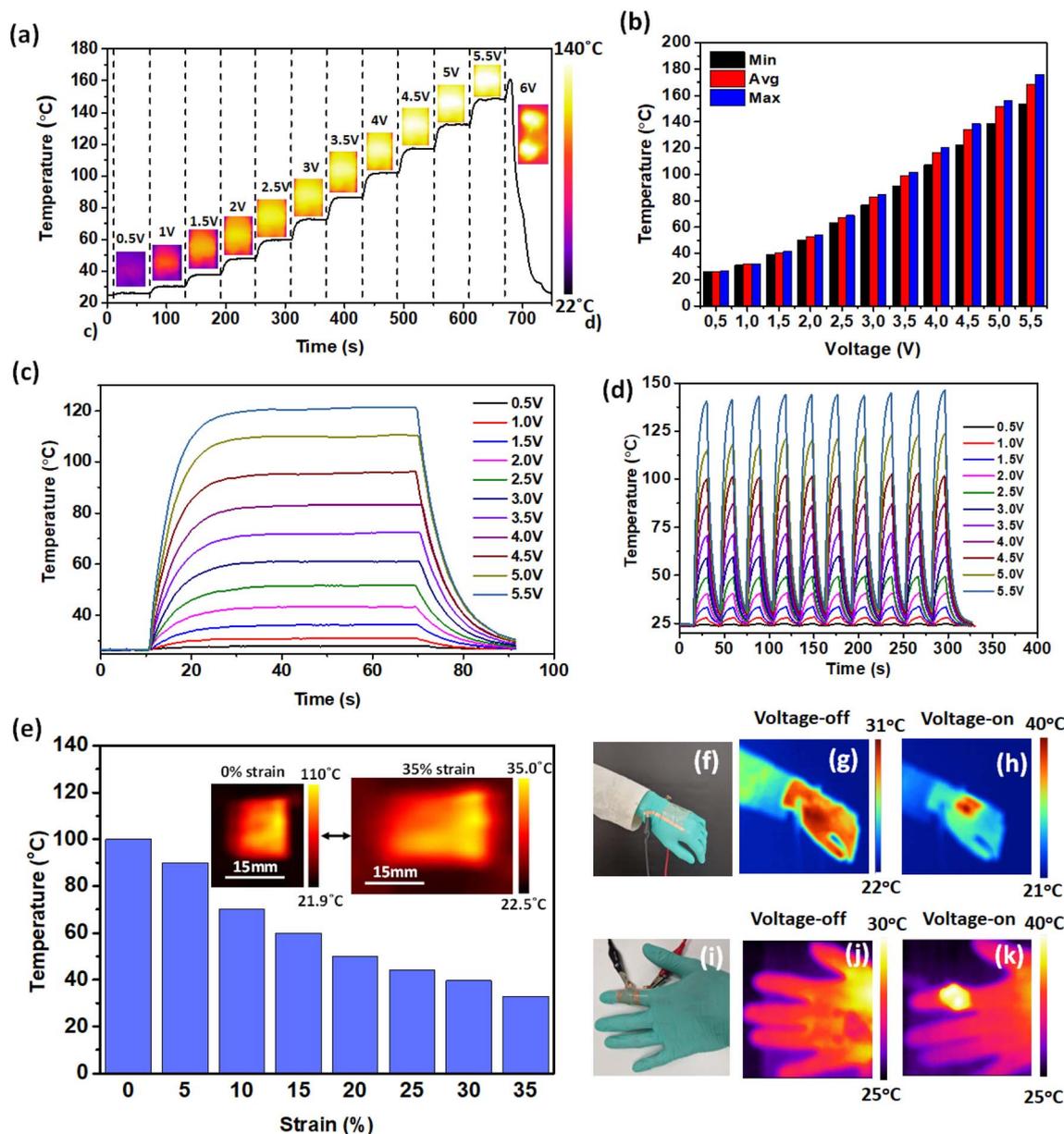Fig. 9 Demonstration of strain sensor mounted on the (a) finger (b) wrist (c) elbow and (d) neck movements.

33188 | J. Mater. Chem. A, 2024, 12, 33177–33192

This journal is © The Royal Society of Chemistry 2024

Fig. 10 Characterization of the PCVU-based heater: (a) heater shows steady-state increase of temperature with the stepwise increase of applied voltage from 0.5 V to 6 V. The corresponding IR images at different applied voltages show the uniform distribution of heat across the heater. (b) Heater shows highest, lowest, and average temperatures measured at different applied voltages (0.5 V to 5.5 V). (c) Time-dependent temperature profile of the heater at different applied voltages for 60 s. (d) Temperature response to voltage on−off studies testing under various voltages (0.5 V to 5.5 V). (e) Temperature response to applied strain from 0−35%, at an applied voltage of 4 V. Demonstration of the flexible heater mounted on (f−h) the wrist and (i−k) the finger, tested under voltage on and off conditions with an applied bias of 2 V.

from 0.5 V to 6 V (increased by 0.5 V every 60 seconds) was applied to the heater until failure (Fig. 10a). The T_s increased consistently with the voltage, reaching a maximum average temperature of ~150 °C at 5.5 V, and the heater failed when the temperature exceeded 160 °C at 6 V. This failure was likely due to the snapping of AgNWs caused by high temperatures at local hotspots near the external connections with copper tapes.[27] The AgNW breakage was attributed to localized heating rather than the applied voltage, as supported by the increase in TCE sheet resistance due to the rise in external heat (Fig. 7c). The heater exhibited uniform heat distribution at different applied

voltages (0.5 V to 6 V), as shown in IR thermal images (Fig. 10a), indicating uniform AgNW distribution across the PCVU substrate. Fig. 10b presents the minimum, average, and highest temperatures recorded at various voltages, demonstrating consistent temperature distribution across the TCE surface. The overall temperature variation, calculated as $(T_{high} - T_{low})/T_{average}$ and found to be ~8.72%, further supports the even distribution of AgNWs across the PCVU substrate.

To check the response time and reliability of our PCVU heater, we recorded a time-dependent temperature profile by monitoring the temperature over time at different applied

This journal is © The Royal Society of Chemistry 2024

J. Mater. Chem. A, 2024, **12**, 33177–33192 | **33189**

voltages from 0.5 V–5.5 V for 60 seconds (Fig. 10c). The surface temperature of the heater increased instantaneously as a function of increasing applied voltage and reached its steady-state operating temperatures in all cases within ~15 s and naturally cooled down within ~15 s once the voltage was turned off (Fig. 10c). These studies underscore its potential use as a flexible transparent heater where rapid heating and cooling are required. Moreover, to assess repeatability, stability, and reliability of the heater, we subjected it to cyclic voltage on-off studies at different applied voltages (0.5 to 5.5 V) for 30 seconds, as shown in Fig. 10d. The heater maintained steady heating and cooling cycles without significant changes in surface heat and response time for different cycles at different applied voltages, confirming its good repeatability and remarkable heating stability.

Additionally, the heater's performance was tested under strain conditions. The strain gradually increased from 5% to 35% while maintaining an applied bias of 4 V (Fig. 10e). Initially, the heater reached a maximum temperature of 100 °C without strain. As the strain increased, the temperature decreased, dropping to 32 °C at 35% strain. Once the strain was released, the heater returned to its original temperature (Video S2, ESI files†). Infrared images showing temperature changes with applied heating are included in Fig. S6, ESI.† The decrease in heater temperature with increasing strain is attributed to the increased resistance of the TCE due to higher junction resistance between the AgNWs under strain. Conversely, minimal strain results in lower junction resistance and higher observed temperatures. These findings highlight the heater's high flexibility and its capability as a stretchable heating element with adjustable temperature.

To assess the stability of our transparent and stretchable heater, a two-month-old heater was tested for its heating characteristics. The aged heater displayed repeatable response times and stability like a fresh heater, as demonstrated by time-dependent temperature profiles and temperature responses to voltage on-off studies performed under applied voltages of 0.5 to 5 V (Fig. S7, ESI†). The heater reached its maximum temperature within 15 s at each applied voltage (0.5 to 5 V) and cooled down naturally within 15 s after the power was turned off in all cases. The heater exhibited stable heating performance at all applied voltages when the voltage was on for 1 minute. Additionally, it showed repeatable heating characteristics when subjected to voltage on-off cycles under applied voltages ranging from 1 V to 5 V. These studies demonstrate that the heater remains stable for at least two months, confirming its good stability, quick response time, repeatable heating characteristics, and reliability.

Finally, the usefulness of our PCVU heater was demonstrated as a thermotherapy pad by mounting it on various body parts such as the wrist and finger and tested by monitoring the surface temperature under voltage on and off conditions (Fig. 10f–k). The heater mounted on the wrist showed a maximum temperature of 31 °C when the voltage was off (Fig. 10g) and reached 40 °C when the voltage was turned-on with an applied bias of 2 V (Fig. 10h). Similarly, when mounted on the finger, the heater displayed a consistent heating pattern. The IR image showed a temperature of 40 °C in the voltage-on state (2 V), compared to 30 °C in the voltage-off state (Fig. 10j and k). These studies conclude that our PCVU based heater is suitable to be used as a wearable thermotherapy heating pad for medical applications.

The overall performance of our PCVU substrate-based heater, featuring rapid response time (~15 s), quick recovery time (~15 s), and achieving high steady-state temperatures (150 °C) at a low driving voltage (5.5 V), was compared with various high-quality heaters using different conductive materials and substrates reported in the literature (Table S2, ESI†). Comparative analysis indicates that our PCVU-based heater stands out as an excellent choice for flexible, transparent, and sustainable heating applications across diverse fields.

4. Conclusion

In conclusion, we have designed, synthesized and characterized a sustainable, castor oil based PCVU elastomeric substrate that exhibits high transmittance (~90%), stretchability (~190%), thermal stability (~210 °C), chemical resistance (non-reactive towards various organic solvents), and good degradability. This substrate was utilized to successfully fabricate a stretchable TCE. The fabrication process involved the use of a PVA nanofabric wet film leveling agent and heat and pressure-based nano-welding techniques, resulting in a TCE that is both mechanically durable and robust with high conductivity and transmittance (50 Ω sq^{-1} and ~75%, respectively, with an AgNWs loading of 111 μg cm^{-2}). The TCE's application was demonstrated in flexible device applications, including a transparent, stretchable strain sensor and a heater. The strain sensor displayed stable resistance changes ($\Delta R/R_0$) for applied strains of 5–15%, with low creep and good repeatability, maintaining signal stability over 100 cycles at 5% strain. The heater achieved a maximum average temperature of ~150 °C at a low voltage of 5.5 V with rapid heating and cooling (15 seconds each). Both the strain sensor and heater were applied in practical applications; the strain sensor was used for real-time human motion detection, monitoring movements such as finger, wrist, elbow and neck flexion cycles, while the heater was implemented as a thermotherapy patch. Considering that breathability is a major concern for polymer-based stretchable devices, our future work will focus on developing sustainable, breathable TCEs for advanced flexible device applications.

Data availability

Additional data supporting this article has been included as part of the ESI.† Data for this article is available at **https://doi.org/10.5281/zenodo.13143510**.

Author contributions

Timo Laukkanen: methodology, formal analysis, data curation, software, formal analysis, data curation. Pulikanti Guruprasad Reddy: methodology, formal analysis, writing – review & editing, writing – original draft, supervision, conceptualization. Amit Barua: validation, methodology, investigation, formal analysis.

33190 | J. Mater. Chem. A, 2024, 12, 33177–33192

This journal is © The Royal Society of Chemistry 2024

Notes and references

1 H. B. Lee, W. Y. Jin, M. M. Ovhal, N. Kumar and J. W. Kang, *J. Mater. Chem. C*, 2019, **7**, 1087–1110.

2 D. Won, J. Bang, S. H. Choi, K. R. Pyun, S. Jeong, Y. Lee and S. H. Ko, *Chem. Rev.*, 2023, **123**, 9982–10078.

3 J. Miao and T. Fan, *Carbon*, 2023, **202**, 495–527.

4 S. Huang, Y. Liu, Y. Zhao, Z. Ren, C. Fei Guo, S. Huang, C. F. Guo, Y. Zhao, Y. Liu and Z. Ren, *Adv. Funct. Mater.*, 2019, **29**, 1805924.

5 D. Li, W.-Y. Lai, Y.-Z. Zhang, W. Huang, D. D. Li, Y. W. Lai, Y.-Z. Zhang and W. Huang, *Adv. Mater.*, 2018, **30**, 1704738.

6 A. Yu, M. Zhu, C. Chen, Y. Li, H. Cui, S. Liu and Q. Zhao, *Adv. Healthcare Mater.*, 2024, **13**, 2302460.

7 X. Yang, W. Chen, Q. Fan, J. Chen, Y. Chen, F. Lai and H. Liu, *Adv. Mater.*, 2024, 2402542.

8 T. Lee, Y. W. Choi, G. Lee, P. V. Pikhitsa, D. Kang, S. M. Kim and M. Choi, *J. Mater. Chem. C*, 2016, **4**, 9947–9953.

9 M.-R. Azani, A. Hassanpour, T. Torres, M.-R. Azani, A. Hassanpour and T. Torres, *Adv. Energy Mater.*, 2020, **10**, 2002536.

10 C. Wang, K. Xia, H. Wang, X. Liang, Z. Yin, Y. Zhang, C. Y. Wang, K. L. Xia, H. M. Wang, X. P. Liang, Z. Yin and Y. Y. Zhang, *Adv. Mater.*, 2019, **31**, 1801072.

11 A. K. Katiyar, A. T. Hoang, D. Xu, J. Hong, B. J. Kim, S. Ji and J. H. Ahn, *Chem. Rev.*, 2024, **124**, 318–419.

12 X. Wu, W. Fu and H. Chen, *ACS Appl. Polym. Mater.*, 2022, **4**, 4609–4623.

13 N. Nasikhudin, Y. Al Fath, I. Istiqomah, H. Rahmadani, M. Diantoro and H. Pujiarti, *Mater. Sci. Forum*, 2024, **1118**, 47–57.

14 W. Li, H. Zhang, S. Shi, J. Xu, X. Qin, Q. He, K. Yang, W. Dai, G. Liu, Q. Zhou, H. Yu, S. R. P. Silva and M. Fahlman, *J. Mater. Chem. C*, 2020, **8**, 4636–4674.

15 Y. Jin, L. Li, Y. Cheng, L. Kong, Q. Pei and F. Xiao, *Adv. Funct. Mater.*, 2015, **25**, 1581–1587.

16 X. Y. Zeng, Q. K. Zhang, R. M. Yu and C. Z. Lu, *Adv. Mater.*, 2010, **22**, 4484–4488.

17 M. S. Miller, J. C. O'Kane, A. Niec, R. S. Carmichael and T. B. Carmichael, *ACS Appl. Mater. Interfaces*, 2013, **5**, 10165–10172.

18 H. Sohn, S. Kim, W. Shin, J. M. Lee, H. Lee, D. J. Yun, K. S. Moon, I. T. Han, C. Kwak and S. J. Hwang, *ACS Appl. Mater. Interfaces*, 2018, **10**, 2688–2700.

19 S. Yu, X. Ma, X. Li, J. Li, B. Gong and X. Wang, *Opt. Mater.*, 2021, **120**, 111414.

20 W. Gaynor, G. F. Burkhard, M. D. McGehee and P. Peumans, *Adv. Mater.*, 2011, **23**, 2905–2910.

21 X. Y. Zeng, Q. K. Zhang, R. M. Yu and C. Z. Lu, *Adv. Mater.*, 2010, **22**, 4484–4488.

22 Y. Ding, Y. Cui, X. Liu, G. Liu and F. Shan, *Appl. Mater. Today*, 2020, **20**, 100634.

23 M. Bian, Y. Qian, H. Cao, T. Huang, Z. Ren, X. Dai, S. Zhang, Y. Qiu, R. Si, L. Yang and S. Yin, *ACS Appl. Mater. Interfaces*, 2023, **15**, 13307–13318.

24 J. S. Meena, S. Bin Choi, S.-B. Jung, J.-W. Kim, J. S. Meena, S. B. Choi, J.-W. Kim and S.-B. Jung, *Adv. Mater. Technol.*, 2023, **8**, 2300602.

25 M. Zarei, G. Lee, S. G. Lee, K. Cho, M. Zarei, S. G. Lee, G. Lee and K. Cho, *Adv. Mater.*, 2023, **35**, 2203193.

26 A. Mousavi, M. Rahimnejad, M. Azimzadeh, M. Akbari and H. Savoji, *J. Mater. Chem. B*, 2023, **11**, 10332–10354.

27 V. Sharma, A. Koivikko, K. Yiannacou, K. Lahtonen and V. Sariola, *npj Flexible Electron.*, 2020, **4**, 1–8.

28 W. Lan, Y. Chen, Z. Yang, W. Han, J. Zhou, Y. Zhang, J. Wang, G. Tang, Y. Wei, W. Dou, Q. Su and E. Xie, *ACS Appl. Mater. Interfaces*, 2017, **9**, 6644–6651.

29 D. T. Papanastasiou, A. Schultheiss, D. Muñoz-Rojas, C. Celle, A. Carella, J.-P. Simonato, D. Bellet, D. T. Papanastasiou, D. Muñoz-Rojas, D. Bellet Univ Grenoble Alpes, A. Schultheiss, C. Celle, A. Carella and J. Simonato, *Adv. Funct. Mater.*, 2020, **30**, 1910225.

30 D. Qi, Z. Liu, W. R. Leow and X. Chen, *MRS Bull.*, 2017, **42**, 103–107.

31 M. Hassan, G. Abbas, N. Li, A. Afzal, Z. Haider, S. Ahmed, X. Xu, C. Pan, Z. Peng, M. Hassan, G. Abbas, N. Li, X. Xu, Z. Peng, A. Afzal, Z. Haider and S. Ahmed, *Adv. Mater. Technol.*, 2022, **7**, 2100773.

32 K.-J. Baeg, J. Lee, J. K. Baeg and J. Lee, *Adv. Mater. Technol.*, 2020, **5**, 2000071.

33 S. S. Murthe, S. Sreekantan and R. B. S. M. N. Mydin, *Polymers*, 2022, **14**, 3267.

34 M. Hassan, G. Abbas, N. Li, A. Afzal, Z. Haider, S. Ahmed, X. Xu, C. Pan and Z. Peng, *Adv. Mater. Technol.*, 2022, **7**, 2100773.

35 R. Yeasmin, S. I. Han, L. T. Duy, B. Ahn and H. Seo, *Chem. Eng. J.*, 2023, **455**, 140543.

36 Y. Yang and H. Zhao, *Appl. Surf. Sci.*, 2022, **577**, 151895.

This journal is © The Royal Society of Chemistry 2024

J. Mater. Chem. A, 2024, **12**, 33177–33192 | **33191**

37 L. Wang, K. Wang, Z. Lou, K. Jiang and G. Shen, *Adv. Funct. Mater.*, 2018, **28**, 1804510.

38 D. Wu, M. Wang, W. Yu, G. G. Wang and J. Zhang, *Chem. Eng. J.*, 2024, **486**, 150121.

39 J. Miao, H. Liu, Y. Li and X. Zhang, *ACS Appl. Mater. Interfaces*, 2018, **10**, 23037–23047.

40 J. W. Chae, D. Lee, A. Osman, B. Kang, J. Hwang, W. Kim, D. Kim, W. H. Lee and S. M. Won, *ACS Appl. Electron. Mater.*, 2024, **6**, 1746–1756.

41 Y. Liu, M. Ahmad, R. A. Venditti, O. D. Velev and Y. Zhu, *Adv. Electron. Mater.*, 2024, **10**, 2300792.

42 S. Chen, Z. Wu, C. Chu, Y. Ni, R. E. Neisiany and Z. You, *Advanced Science*, 2022, **9**, 2105146.

43 Z. Yang, S. Zhang, Z. Chen, X. Lai, H. Li and X. Zeng, *ACS Appl. Polym. Mater.*, 2024, **6**, 905–914.

44 A. K. Brooks, S. Pradhan and V. K. Yadavalli, *ACS Appl. Bio. Mater.*, 2023, **6**, 4392–4402.

45 S. Chen, L. Sun, X. Zhou, Y. Guo, J. Song, S. Qian, Z. Liu, Q. Guan, E. Meade Jeffries, W. Liu, Y. Wang, C. He and Z. You, *Nat. Commun.*, 2020, **11**, 1–8.

46 L. Zhang, J. Liang, C. Jiang, Z. Liu, L. Sun, S. Chen, H. Xuan, D. Lei, Q. Guan, X. Ye and Z. You, *Natl. Sci. Rev.*, 2021, **8**, 2021.

47 B. L. Turner, J. Twiddy, M. D. Wilkins, S. Ramesh, K. M. Kilgour, E. Domingos, O. Nasrallah, S. Menegatti and M. A. Daniele, *npj Flexible Electronics*, 2023, **7**, 1–14.

48 I. Haider, M. Mosallaei, K. Yiannacou, A. Vehkaoja, S. Zakeri, V. Sariola and V. Sharma, *Adv. Eng. Mater.*, 2023, **25**, 2201172.

49 A. Elsayes, V. Sharma, K. Yiannacou, A. Koivikko, A. Rasheed, V. Sariola, A. Elsayes, V. Sharma, K. Yiannacou, A. Koivikko, A. Rasheed and V. Sariola, *Adv. Sustainable Syst.*, 2020, **4**, 2000056.

50 P. Guruprasad Reddy, A. Barua, T. Laukkanen, B. Mostafiz, T. Tirri, A. Vainio and V. Sharma, *Chem. Eng. J.*, 2024, **495**, 153531.

51 A. Costa Cornellà, S. K. Tabrizian, P. Ferrentino, E. Roels, S. Terryn, B. Vanderborght, G. Van Assche and J. Brancart, *ACS Sustain. Chem. Eng.*, 2023, **11**, 3437–3450.

52 M. J. L. Tschan, E. Brulé, P. Haquette and C. M. Thomas, *Polym. Chem.*, 2012, **3**, 836–851.

53 H. Huang, H. Pang, J. Huang, P. Yu, J. Li, M. Lu and B. Liao, *Constr. Build. Mater.*, 2021, **284**, 122388.

54 L. Xue, S. Dai and Z. Li, *Macromolecules*, 2009, **42**, 964–972.

55 S.-H. Hsiao, PhD thesis, Kyoto University, Japan, 2008, **https://repository.kulib.kyoto-u.ac.jp/dspace/handle/2433/57295?mode=full**.

56 H. jiang Ni, J. gang Liu, Z. he Wang and S. yong Yang, *J. Ind. Eng. Chem.*, 2015, **28**, 16–27.

57 Y. Taketani, K. Iwata, H. Nitta, U. Yonemura and T. Sasaki, *US Pat.*, 5561180, 1996.

58 J. W. Leem, S. Kim, S. H. Lee, J. A. Rogers, E. Kim and J. S. Yu, *Adv. Energy Mater.*, 2014, **4**, 1301315.

59 J. Liang, L. Li, X. Niu, Z. Yu and Q. Pei, *Nat. Photonics*, 2013, **7**, 817–824.

60 W. B. Han, G. J. Ko, K. G. Lee, D. Kim, J. H. Lee, S. M. Yang, D. J. Kim, J. W. Shin, T. M. Jang, S. Han, H. Zhou, H. Kang, J. H. Lim, K. Rajaram, H. Cheng, Y. D. Park, S. H. Kim and S. W. Hwang, *Nat. Commun.*, 2023, **14**, 1–12.

61 Q. Hua, Z. Huang, J. Gou, H. Zhang, I. Therrien, J. Wu, Y. Liang and S. Renneckar, *Chem. Eng. J.*, 2024, **499**, 156139.

62 A. Bowen, J. Li, J. Lewis, K. Sivaramakrishnan, T. L. Alford and S. Iyer, *Thin Solid Films*, 2011, **519**, 1809–1816.

63 S. J. Mostafavi Yazdi and J. Baqersad, *J. Biomech.*, 2022, **130**, 110864.

64 R. Yeasmin, S. I. Han, L. T. Duy, B. Ahn and H. Seo, *Chem. Eng. J.*, 2023, **455**, 140543.

65 J. Liu, H. Zheng, P. S. P. Poh, H. G. Machens and A. F. Schilling, *Int. J. Mol. Sci.*, 2015, **16**, 15997–16016.

66 Z. Yang, S. Zhang, Z. Chen, X. Lai, H. Li and X. Zeng, *ACS Appl. Polym. Mater.*, 2024, **6**, 905–914.

67 D. Pei, C. An, B. Zhao, M. Ge, Z. Wang, W. Dong, C. Wang, Y. Deng, D. Song, Z. Ma, Y. Han and Y. Geng, *ACS Appl. Mater. Interfaces*, 2022, **14**, 33806–33816.

68 P. Cai, B. Hu, W. R. Leow, X. Wang, X. J. Loh, Y. L. Wu and X. Chen, *Adv. Mater.*, 2018, **30**, 1800572.

69 E. J. Kappert, M. J. T. Raaijmakers, K. Tempelman, F. P. Cuperus, W. Ogieglo and N. E. Benes, *J. Membr. Sci.*, 2019, **569**, 177–199.

70 Y. Yang and H. Zhao, *Appl. Surf. Sci.*, 2022, **577**, 151895.

71 V. J. Parekh, V. K. Rathod and A. B. Pandit, *Comprehensive Biotechnology*, 2nd edn, 2011, vol. 2, pp. 103–118.

72 P. Guruprasad Reddy and A. J. Domb, *Polym. Adv. Technol.*, 2021, **32**, 3835–3856.

73 World Health Organization (WHO) online, **https://cdn.who.int/media/docs/default-source/wash-documents/wash-chemicals/ph.pdf?sfvrsn=16b10656_4**, accessed October 2024.

74 V. Sharma, K. Yiannacou, M. Karjalainen, K. Lahtonen, M. Valden and V. Sariola, *Nanoscale Adv.*, 2019, **1**, 4025–4040.

75 X. Yu, X. Yu, J. Zhang, D. Zhang, J. Ni, H. Cai, D. Zhang and Y. Zhao, *Mater. Lett.*, 2015, **145**, 219–223.

76 C. Y. Leong, S. S. Yap, G. L. Ong, T. S. Ong, S. L. Yap, Y. T. Chin, S. F. Lee, T. Y. Tou and C. H. Nee, *Nanotechnol. Rev.*, 2020, **9**, 1539–1549.

77 C. L. Kim, J. Y. Lee, D. G. Shin, J. S. Yeo and D. E. Kim, *Sci. Rep.*, 2020, **10**, 1–8.

78 D. Kim, S. H. Kim, J. H. Kim, J. C. Lee, J. P. Ahn and S. W. Kim, *Sci. Rep.*, 2017, **7**, 1–8.

79 D. T. Papanastasiou, A. Schultheiss, D. Muñoz-Rojas, C. Celle, A. Carella, J. P. Simonato and D. Bellet, *Adv. Funct. Mater.*, 2020, **30**, 1910225.

33192 | *J. Mater. Chem. A*, 2024, **12**, 33177–33192

This journal is © The Royal Society of Chemistry 2024